Proceedings of the Canadian Society for Mechanical Engineering International Congress
32nd Annual Conference of the Computational Fluid Dynamics Society of Canada
Canadian Society of Rheology Symposium
CSME-CFDSC-CSR 2025
May 25–28, 2025, Montréal, Québec, Canada

Investigating wake dynamics around airfoils with varying slip lengths using proper orthogonal decomposition

Emmanuel Quayson-Sackey[1]*, Eugene Kankam[1], Baafour Nyantekyi-Kwakye[1], Mohammad Saeedi[1], Ehsan Asgari[1]
[1] Mechanical Engineering, Dalhousie University, Halifax, Canada
*em643097@dal.ca

Abstract- The present article investigates wake dynamics around a NACA 64-618 airfoil with varying slip lengths using proper orthogonal decomposition. The Navier slip boundary condition was utilized to mimic the slip effect imposed by superhydrophobic coating in real conditions. Mean velocities, and evolution of turbulent structures in the wake region were examined thoroughly. It was observed that increasing slip length on the surface of the airfoil delays flow separation, reduces the recirculation bubble size formed at the trailing edge and alters vortex dynamics in the wake region. Proper orthogonal decomposition also revealed that the fractional energy of the first mode increases over the slip surface compared to the no slip surface.

Keywords- Turbulence; drag reduction; proper orthogonal decomposition; airfoil

I. INTRODUCTION

Drag reduction on surfaces has been a focal point of research over the past decade due to its critical role in fluid dynamics, particularly in flow control, ice mitigation and efficiency enhancement [1]. A wide range of drag reduction techniques have been developed in recent years and broadly categorized into active and passive control strategies. Passive control strategies including superhydrophobic coatings (SHC) and the use of riblets have received substantial attention due to their ability to achieve drag reduction without requiring continuous energy input [2].

The SHC inspired by the lotus leaf has been attracting attention due to its remarkable viscous drag reduction, self-cleaning, anticorrosion, and anti-icing properties. Superhydrophobic coated surfaces leverage their intrinsic properties such as high-water contact angle ($\theta > 150°$), nano/microscale level surface roughness and low contact angle hysteresis to repel water droplets by facilitating rapid droplet movement across surfaces [3]. Researchers attribute this acceleration to the presence of trapped air within the grooves of the micro-nano rough structures. This trapped air creates an air-water interface, reducing skin friction drag and enhancing the movement of fluids [4]. The slip effect is normally quantified using the slip length (L_s), which ranges on the scale of hundreds of micrometers. The slip length represents the fictitious distance beneath the slipping surface where the fluid velocity linearly extrapolates linearly to zero, effectively characterizing the magnitude of slippage at the boundary [5].

Given the significance of SHC as explained above, research on flow dynamics over these surfaces has gained substantial interest in the past decade. This growing attention is driven by the need to address key challenges, including flow separation, recirculation bubble size, shear layer instability, and understanding the evolution of turbulent structures in the wake region [6]. Consequently, extensive studies have been conducted both experimentally and numerically. Wang et al. [7] utilized time-resolved particle image velocimetry (TRPIV) to investigate the effect of slip wall on drag and coherent structures over a superhydrophobic surface (SHS). They observed that the dynamics of coherent structures in the turbulent boundary layer changes when the slip velocity over the SHS decreases the velocity gradient. Sooraj et al. [8] investigated the influence of SHS on the wake dynamics around a circular cylinder using PIV. Their results depicted that the onset of vortex shedding was delayed, while early rolling-up of vortices were accelerated, resulting in reduced recirculation lengths in unsteady regimes. Also, the velocity deficit experienced by the superhydrophobic cylinder wake was comparatively less and the effect was more profound in the Reynolds number (Re) range 300–860. Furthermore, proper orthogonal decomposition (POD) was used to examine the wake coherent structure. A larger number of coherent structures and change in vortex shedding pattern to primary and secondary vortices were observed in the near wake of the superhydrophobic cylinder.

As can be seen from the literature, a wide range of experimental work has been conducted to investigate drag reduction, vortex propagation and turbulent structures around SHS. However, their validity is limited by measurement inaccuracies and resolution constraints leading to inconsistencies in results. To address these uncertainties, several numerical studies have been conducted to provide comprehensive understanding of the flow characteristics and

vortex dynamics around SHS. Legendre et al. [9] investigated the influence of generic slip boundary condition on the wake dynamics around a two-dimensional (2D) flow past a circular cylinder using a finite volume numerical code. They observed that slip significantly delays the onset of recirculation and shedding in the wake behind the cylinder. You and Moin [10] numerically studied the effects of hydrophobic surfaces on the drag and lift of a circular cylinder using direct numerical simulation and large-eddy simulations at Re of 300 and 3900. They observed a reduction in both the mean drag and the root-mean-square lift coefficient values. Also, the drag reduction in the laminar vortex shedding regime was primarily attributed to a decrease in skin friction, whereas in the shear layer transition regime, the reduction was mainly due to a delay in flow separation.

Information from the literature shows that extensive research has been conducted to explore the effects of superhydrophobicity on hydrofoils. However, their unsteady effects on non-symmetric airfoils have not been extensively investigated and fully understood as more complex flow phenomena such as flow separation delay, vortex shedding, and changes in aerodynamic characteristics can occur due to the surface curvature of the airfoil and varying slip lengths. To address this gap, the present numerical study aims to investigate the wake dynamics around NACA 64-618 airfoil with varying slip lengths using proper orthogonal decomposition.

II. SIMULATION SETUP

A. Governing equations and numerical algorithms

The incompressible viscous flow around the 2D NACA 64-618 airfoil was simulated using the finite volume method to discretize and solve the Reynolds-averaged Navier–Stokes (RANS) equations. The governing equations for the mass and momentum conservation are written as:

$$\frac{\partial u_i}{\partial x_i} = 0\,, \tag{1}$$

$$\frac{\partial}{\partial t}(\rho u_i) + \frac{\partial}{\partial x_j}(\rho u_i u_j) = -\frac{\partial p}{\partial x_i} + \frac{\partial}{\partial x_j}\left[\mu\left(\frac{\partial u_i}{\partial x_j} + \frac{\partial u_j}{\partial x_i}\right)\right] + \frac{\partial}{\partial x_j}\left(-\overline{\rho u_i' u_j'}\right), \tag{2}$$

where x_i (i = 1, 2, 3) represents the cartesian coordinates, u_i are the corresponding velocity components, p is the pressure, ρ is the density, μ is the dynamic viscosity and $-\overline{\rho u_i' u_j'}$ are the Reynolds stresses.

To model the turbulent flow around the airfoil, the one-equation intermittency factor γ based transition model coupled with the shear stress transport (SST) k–ω model is adopted in the simulation. The SST k–ω model is developed with the combination of the k–ε model and the k–ω model through a blending function and retains the advantages of the k–ε model in the free stream and the k–ω model for low Reynolds number and near the wall boundary layer. It makes the adopted model applicable to a broad range of flows including the complex flows with adverse pressure gradients and boundary layer separation [11]. Furthermore, the SST γ model coupling the γ model and the SST k–ω model has been adopted and validated by many researchers in transition modeling, which has shown good correlation with experiments, and is therefore adopted in the present simulation [12]. The transport equation for the intermittency factor γ takes the following form:

$$\frac{\partial(\rho\gamma)}{\partial t} + \frac{\partial(\rho u_j \gamma)}{\partial x_j} = P_\gamma - E_\gamma + \frac{\partial}{\partial x_j}\left[\left(\mu + \frac{\mu_t}{\sigma_\gamma}\right)\frac{\partial \gamma}{\partial x_j}\right], \tag{3}$$

where P_γ and E_γ denote the transition source term and destruction term, respectively. They are expressed as:

$$P_\gamma = F_{\text{length}}\rho S\gamma(1-\gamma)F_{\text{onset}}\,, \tag{4}$$

$$E_\gamma = C_{a2}\rho\Omega\,\gamma F_{\text{turb}}(C_{e2}\gamma - 1), \tag{5}$$

where S is the strain rate magnitude, and Ω is the magnitude of the absolute vorticity rate. The values of the model constants F_{length}, C_{a2}, C_{e2}, σ_γ and are 100, 0.06, 50, and 1.0, respectively. More details about the model functions (F_{onset} and F_{turb}) can be referred to Menter et al. [13]

All numerical simulations were performed using ANSYS FLUENT 2024 R1. The simulations were conducted utilizing a second-order implicit temporal scheme to ensure enhanced accuracy in capturing time-dependent flow dynamics. Spatial terms discretization utilized a second-order upwind scheme to minimize numerical diffusion and improve the resolution of flow structures. Pressure-velocity coupling was performed by the SIMPLE algorithm ensuring robust convergence for the incompressible flow solver. The time step size was set to Δt = 3×10^{-4} s. To maintain numerical stability and accuracy, the maximum Courant-Friedrichs-Lewy (CFL= $U\Delta t/\Delta x$) number was constrained to 1 throughout the simulation. The convergence criterion for solving the momentum and continuity (Poisson) equations was defined as 1×10^{-6} based on the maximum residual difference in each velocity component. All the computations were performed using a high-performance computing cluster (Beluga) based on Intel Gold 6148 Skylake 2.4 GHz chip technology. The total computing time spent on solving the flow field and collecting the statistics was about 300 CPU hours. Before the flow statistics are collected, it is important to ensure that the flow has reached a statistically stationary state. In this present study, the simulation was first run for approximately 10 flow-through pass to allow the flow field to fully evolve to a statistically stationary state. Then the flow statistics were collected through a course of approximately 5.5 flow-through pass.

B. Test case, grid generation and boundary conditions

The research utilized the NACA 64-618 airfoil which is typically located at the tip section of NREL 5MW baseline OWT blade [14]. This is a 6-series airfoil with maximum thickness of 18 % located at 34.7 % of the chord from the leading edge and a maximum camber of 3.3% at 50% of the chord. The airfoil has a chord length, c = 1 m located at the

center of the computational domain as shown in Fig. 1(a). The domain extends 10*c* upstream from the airfoil leading edge, 22*c* downstream from the leading edge and spans ± 10*c* in the wall-normal direction. This flow domain was used for the simulation to accurately capture wake development, vortex shedding and prevent flow reversal at the outlet. The domain was discretized using a fully structured *C*-type mesh around the airfoil as illustrated in Fig. 1(b). As shown in the close-up view, the mesh maintains good orthogonality near the airfoil surface for accurate boundary layer resolution. To capture regions with high velocity gradients and strong shear forces on the wall of the airfoil, the first node was placed 0.002 mm from the boundary ensuring a dimensionless wall distance (y^+) of less than 1. The growth ratio of the cells away from the wall was 1.2 times greater in size than the node before. To ensure grid adequacy, a grid independence study was conducted, and the final mesh consists of approximately 750 ×10^3 cells.

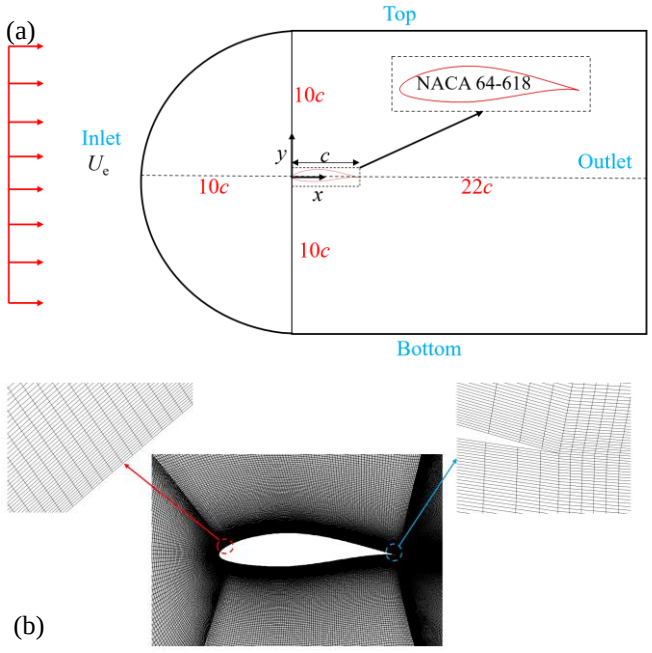

Figure 1. Schematic diagram of the (a) computational domain and (b) mesh distribution around the airfoil model.

Air at 15 ℃ with density of ρ_{air} = 1.225 kgm^{-3} and constant dynamic viscosity of μ_{air} = 1.789 × 10^{-5} Pa/s was used as a working fluid for the simulation. In terms of boundary conditions, a Dirichlet boundary condition prescribing a uniform velocity, U_e = 20 m/s was applied at the inlet, while a constant relative pressure of 0 Pa was imposed at the outlet. Symmetry conditions were also applied at the top and bottom surfaces of the computational domain. Since the focus of this study is to investigate the effect of slip on the wake dynamics of the airfoil at α =12°, two boundary conditions were used. Initially, a no-slip boundary condition was assigned to the wall surfaces, specifying zero velocity at the fluid-solid interface. Consequently, a slip surface boundary condition was modeled on the wall using the Navier slip boundary condition as shown in Eq. (6) to assume a SHS [15].

$$U_s = L_s \frac{\partial U}{\partial n}\Big|_{wall} \tag{6}$$

As shown in Eq. (6), U_s at each cell on the airfoil surface can be obtained by multiplying the tangential velocity gradient term with the given L_s value. As a result, a UDF script was written and compiled using the in-built compiler in FLUENT software. It is interesting to note that the U_s on the surface was obtained by iteratively executing the above equation with low relaxation factor in each iteration. The U_s obtained was used to modify the airfoil wall boundary condition in the software.

III. RESULTS AND DISCUSSION

A. *Validation*

Since no direct reference data is available for the coated NACA 64-618 airfoil, a comparative analysis was conducted using published results for the non-coated airfoil [16]. The comparison focuses on the mean pressure coefficient (C_p) distribution along the airfoil at $\alpha = -0.88°$. Fig. 2(a) illustrates the variation of C_p along the normalized chord length (x/c) at $\alpha = -0.88°$. The numerical results from the present study show good agreement with experimental data across most of the chord length. However, a small discrepancy is observed in the suction region near the airfoil's upper surface (x/c = 0.6) where the numerical prediction slightly underestimates with a relative error of approximately 15%. This may be attributed to limitations in the turbulence modeling approach in capturing

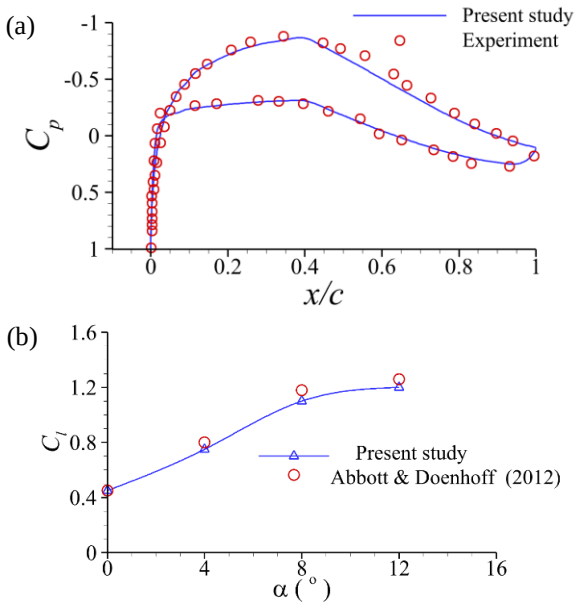

Figure 2. Comparison of (a) mean pressure and (b) lift coefficient of the present study with experimental data for no-slip boundary condition.

complex boundary layer interactions in this region. Figure 2(b) represents the variation of C_l as a function of α. The numerical predictions align closely with the wind tunnel results from Abbott and Doenhoff [17] demonstrating a consistent trend across the range of angles considered. The lift coefficient

increases steadily with α, with a noticeable nonlinear growth at higher angles, particularly near $\alpha = 12°$. This behavior indicates the onset of flow separation effects at high α, which are well captured by the present numerical approach. The overall agreement between the numerical and experimental results confirms the reliability and accuracy of the simulation framework for further analysis.

B. *Mean flow field*

Figure 3 depicts the contours of the normalized streamwise mean velocities (U/U_e) for all test cases. Generally, the flow topology revealed flow deceleration at the leading edge, acceleration at the suction surface of the airfoil and separation at the trailing edge due to adverse pressure gradient formed by the upstream flowing fluid. For the no-slip case as shown in Fig.3 (a), a distinct reverse flow region ($U < 0$) demarcated by the zero-contour line ($U = 0$) is observed at the suction surface near trailing edge. This can clearly be seen from the mean streamlines which reveal a recirculation bubble characterized by counterclockwise rotating vortices.

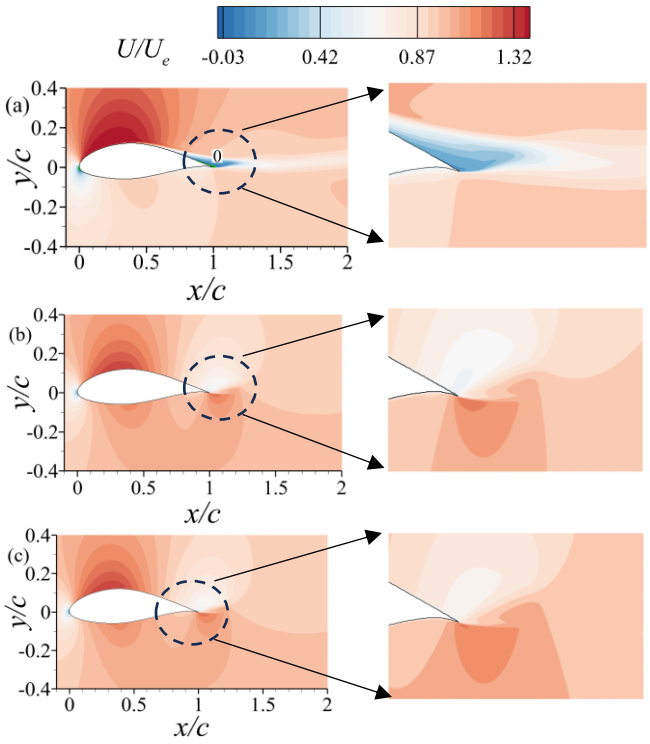

Figure 3. Contours of mean streamwise velocities for (a) no-slip (b) L_s = 100 μm and (c) L_s = 185 μm. Contours to the right-hand side of (a), (b) and (c) represent zoomed-in section of the trailing edge and separation bubble

However, it is interesting to note that the boundary layer remains attached to the surface for the SHC as shown in Fig.3 (b) and Fig.3 (c). This can be attributed to the fact that, the slip possibly induces a non-zero slip velocity which overcomes the adverse pressure gradient thereby enhancing the suppression of the recirculation bubble. Also, compared to the no-slip case, flow acceleration and faster velocity recovery in the wake region for the slip surfaces were observed. This is due to the continual entrainment of ambient fluid into the core of the wake region, allowing faster recovery of the mean flow. To further understand the wake dynamics, the wake formation lengths (L_w/c) measured from the trailing edge of the airfoil to the point where the velocity recovers to approximately 95% of the freestream velocity were assessed. Specifically, the wake formation length was measured as L_w/c = 6.0, 0.70 and 0.31 for no-slip, L_s = 100μm and L_s = 185μm, respectively. Notably, a significant reduction in the wake formation length was observed as the slip length increased. This can be attributed to the reduction in the size of the recirculation bubble and the suppression of the flow separation.

C. *Proper orthogonal decomposition analysis*

To gain better insight into the development of large-scale coherent structures in the wake flow, POD of the streamwise fluctuating velocities were performed for the no-slip and all slip conditions. In this text, only no-slip and L_s = 185 μm are shown due to space limitation. POD provides the optimal approximation of the total turbulent kinetic energy within a specified number of modes. It organizes these modes in descending order of their energy contribution, ensuring that the first mode captures the highest amount of energy. Since its introduction, the POD technique has been applied to investigate coherent structures in turbulent jet flows [18] and separated flows [8]. In the present study, the snapshot method proposed by Sirovich [19] was used to decompose the fluctuating velocity vector field $u'(\boldsymbol{x}, t)$ into a combination of spatial modes and their respective temporal coefficients as shown in Eq. (7).

$$u(\boldsymbol{x}, t) = \sum_{n=1}^{N} a_n(t)\Phi_n(\boldsymbol{x}) \tag{7}$$

where N is the number of snapshots, Φ_n are the spatial POD mode magnitude and a_n(t) the temporal coefficients for the modes. The time step chosen for the simulation was utilized to collect the POD snapshots, ensuring the capture of high-frequency structures in the wake flow. Since the accuracy of the POD analysis is dependent on the number of snapshots, a convergence of the POD results was evaluated by computing the fractional turbulent kinetic energy associated with the first mode for increasing N. Results of the energy convergence for all test cases were qualitatively similar. The energy fraction for the first mode decreased with increasing N until a threshold value was attained where the fractional energy became independent of N. For instance, in all cases, increasing N from 2500 to 3000 yielded fractional turbulent kinetic energy errors of 5.1%, 2.7% and 2.6% for no-slip, L_s = 100 μm and L_s = 185 μm respectively as shown in Table 1. Based on these observations, it was determined that N = 3000 was sufficient to perform the POD analysis.

Figure 4 shows fractional energy contribution over the first 20 POD modes for the no-slip, L_s = 100 μm and L_s = 185 μm. From Fig. 4, the first mode contributed 9.9%, 11.3% and 11.8% of the total energy for no-slip, L_s = 100 μm and L_s = 185 μm respectively. The increase in fractional energy for the first mode suggests that the flow becomes more organized with greater proportion of turbulent kinetic energy associated with large-

scale coherent motions. The formation of these coherent structures can be associated with the reduction of wall shear stress on the boundary facilitated by the slip effect. This finding supports the notion that slip generally modifies the dissipative small scales close to the surface while promoting the formation of organized coherent large-scale structures. These findings align with earlier work by Sooraj et al. [8] despite difference in Re and energy content.

TABLE I. CONVERGENCE TEST OF DIFFERENT SNAPSHOTS FOR NO-SLIP, L_S = 100 μm AND L_S = 185 μm

Snapshots	**Energy content**		
	No-slip	**100 μm**	**185 μm**
100	0.191	0.159	0.217
500	0.111	0.117	0.109
1000	0.113	0.118	0.107
1500	0.107	0.111	0.115
2000	0.102	0.105	0.116
2500	0.103	0.110	0.113
3000	0.098	0.113	0.116

To show a typical pattern and the flow behavior associated with the convective structures in the wake, Fig. 5 and 6 displays the first three spatial POD modes for no-slip and L_s = 185 μm. For both cases, the first two modes, $\Phi_1{}^u$ and $\Phi_2{}^u$, exhibit alternating spatial convective flow structures within the wake region. The first two modes form a mode pair, with a phase shift of approximately $\lambda/2$ in the streamwise direction, indicating their role in representing the primary oscillatory behavior of the wake. The third POD mode, $\Phi_3{}^u$, represents higher-order flow structures that contribute to secondary instabilities in the wake. In both no-slip and slip cases, this mode appears more localized near the trailing edge, capturing smaller-scale fluctuations. However, in the slip case, the intensity of this mode is slightly diminished, indicating that slip conditions dampen smaller-scale turbulence in the near wake region. This reduction suggests that the slip condition alters the energy cascade by altering the generation of higher-frequency modes as discussed earlier.

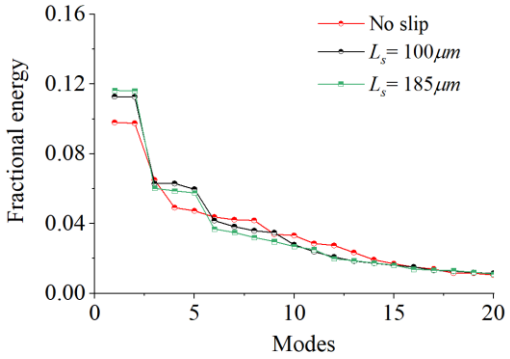

Figure 4. Fractional mode energy distribution for the no-slip, L_s = 100 μm and L_s = 185 μm

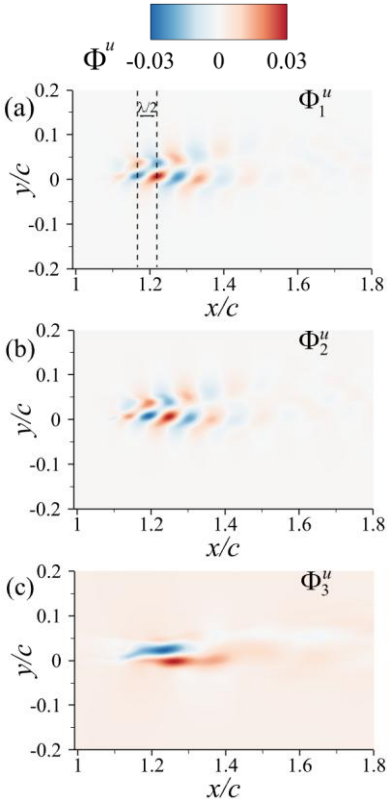

Figure 5. Decomposed streamwise convective structures in the wake region of the no-slip case: (a) mode 1 (b) mode 2 (c) mode 3

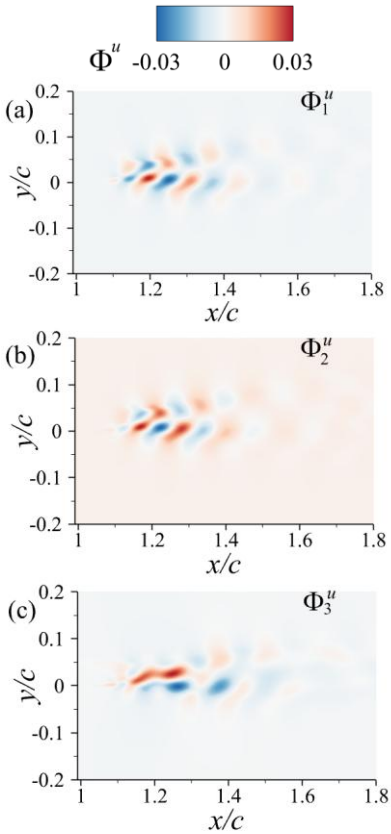

Figure 6: Decomposed streamwise convective structures in the wake region of the slip (L_s = 185 μm) case: (a) mode 1 (b) mode 2 (c) mode 3

IV. CONCLUSION

A parametric study is conducted on superhydrophobic surfaces and a smooth (no-slip) airfoil over a large Reynolds number. The objective of the study is to understand the effect of superhydrophobicity on the mean flow field and the wake dynamics around the airfoil. Time averaged flow fields and coherent structures in the wake were thoroughly examined using POD. The results revealed that the imposition of slip on the airfoil surface effectively suppressed flow separation at the trailing edge. Additionally, the slip condition enhanced the entrainment of ambient fluid within the wake, leading to an accelerated velocity recovery downstream the airfoil. The POD analysis further revealed that the fractional turbulent kinetic energy captured by the first mode increased with slip length, suggesting that SHC promotes the formation of dominant coherent structures in the wake. As a future work, different slip lengths will be examined to understand the underlying physics of this subject.

ACKNOWLEDGMENT

The authors acknowledge financial support from National Sciences and Engineering Research Council of Canada Discovery grant (RGPIN-2024-04606) awarded to BN-K and the support of Digital Research Alliance of Canada.

REFERENCES

[1] Quayson-Sackey, E., Nyantekyi-Kwakye, B., and Ayetor, G. K., 2024, "Technological Advancements for Anti-Icing and de-Icing Offshore Wind Turbine Blades," Cold Reg Sci Technol, p. 104400.

[2] Sooraj, P., Jain, S., and Agrawal, A., 2019, "Flow over Hydrofoils with Varying Hydrophobicity," Exp Therm Fluid Sci, 102, pp. 479–492.

[3] Li, W., Zhan, Y., and Yu, S., 2021, "Applications of Superhydrophobic Coatings in Anti-Icing: Theory, Mechanisms, Impact Factors, Challenges and Perspectives," Prog Org Coat, 152, p. 106117. https://doi.org/https://doi.org/10.1016/j.porgcoat.2020.106117.

[4] Samaha, M. A., and Gad-el-Hak, M., 2021, "Slippery Surfaces: A Decade of Progress," Physics of Fluids, 33(7).

[5] Rastan, M. R., Foshat, S., and Sekhavat, S., 2019, "High-Reynolds Number Flow around Coated Symmetrical Hydrofoil: Effect of Streamwise Slip on Drag Force and Vortex Structures," J Mar Sci Technol, 24, pp. 500–511.

[6] Shahsavari, A., Nejat, A., Climent, E., and Chini, S. F., 2023, "Unexpected Trends of Lift for Hydrofoils with Superhydrophobic Coating," European Journal of Mechanics - B/Fluids, 101, pp. 219–226. https://doi.org/https://doi.org/10.1016/j.euromechflu.2023.05.004.

[7] Wang, X., Wang, Y., Tian, H., and Jiang, N., 2021, "Effects of the Slip Wall on the Drag and Coherent Structures of Turbulent Boundary Layer," Acta Mechanica Sinica/Lixue Xuebao, 37(8), pp. 1278–1290. https://doi.org/10.1007/s10409-021-01092-0.

[8] Sooraj, P., Ramagya, M. S., Khan, M. H., Sharma, A., and Agrawal, A., 2020, "Effect of Superhydrophobicity on the Flow Past a Circular Cylinder in Various Flow Regimes," J Fluid Mech, 897, p. A21.

[9] Legendre, D., Lauga, E., and Magnaudet, J., 2009, "Influence of Slip on the Dynamics of Two-Dimensional Wakes," J Fluid Mech, 633, pp. 437–447.

[10] You, D., and Moin, P., 2007, "Effects of Hydrophobic Surfaces on the Drag and Lift of a Circular Cylinder," Physics of Fluids, 19(8).

[11] Zhu, M., Huang, W., Ma, L., and Luo, J., 2024, "Influence of Surface Slip on Hydrodynamics and Flow Field around a Two-Dimensional Hydrofoil at a Moderate Reynolds Number," Physics of Fluids, 36(5).

[12] Liu, Y., Li, P., and Jiang, K., 2021, "Comparative Assessment of Transitional Turbulence Models for Airfoil Aerodynamics in the Low Reynolds Number Range," Journal of Wind Engineering and Industrial Aerodynamics, 217, p. 104726.

[13] Menter, F. R., Smirnov, P. E., Liu, T., and Avancha, R., 2015, "A One-Equation Local Correlation-Based Transition Model," Flow Turbul Combust, 95, pp. 583–619.

[14] Jonkman, J., 2009, "Definition of a 5-MW Reference Wind Turbine for Offshore System Development," National Renewable Energy Laboratory.

[15] Navier, C., 1822, *Mémoire Sur Les Lois Du Mouvement Des Fluides*, éditeur inconnu.

[16] Romani, G., van der Velden, W. C., and Casalino, D., 2018, "Deterministic and Statistical Analysis of Trailing-Edge Noise Mechanisms with and without Serrations," *2018 AIAA/CEAS Aeroacoustics Conference*, p. 3129.

[17] Abbott, I. H., and Von Doenhoff, A. E., 2012, *Theory of Wing Sections: Including a Summary of Airfoil Data*, Courier Corporation.

[18] Nyantekyi-Kwakye, B., Tachie, M. F., and Clark, S. P., 2016, "Flow Characteristics of an Offset Jet over a Surface Mounted Square Rib," Journal of Turbulence, 17(8), pp. 727–757.

[19] Sirovich, L., 1987, "Turbulence and the Dynamics of Coherent Structure. Part i, Ii, Iii," Quat. Appl. Math., 3, p. 583.